Crystal structures and X-ray powder diffraction data for Cs2NiSi5O12, RbGaSi2O6, and CsGaSi2O6 synthetic leucite analogues

BELL, Anthony and STONE, Alex

Crystal structures and X-ray powder diffraction data for $Cs_2NiSi_5O_{12}$, $RbGaSi_2O_6$, and $CsGaSi_2O_6$ synthetic leucite analogues

Anthony M. T. Bell [a] and Alex H. Stone
Materials and Engineering Research Institute, Sheffield Hallam University, Sheffield S1 1WB, UK

(Received 21 July 2021; accepted 17 September 2021)

Leucites are tetrahedrally coordinated silicate framework structures with some of the silicon framework cations partially replaced by divalent or trivalent cations. These structures have general formulae $A_2BSi_5O_{12}$ and $ACSi_2O_6$; where A is a monovalent alkali metal cation, B is a divalent cation, and C is a trivalent cation. In this paper, we report the Rietveld refinements of three more synthetic leucite analogues with stoichiometries of $Cs_2NiSi_5O_{12}$, $RbGaSi_2O_6$, and $CsGaSi_2O_6$. $Cs_2NiSi_5O_{12}$ is $Ia\bar{3}d$ cubic and is isostructural with $Cs_2CuSi_5O_{12}$. $RbGaSi_2O_6$ is $I4_1/a$ tetragonal and is isostructural with $KGaSi_2O_6$. $CsGaSi_2O_6$ is $I\bar{4}3d$ cubic and is isostructural with $RbBSi_2O_6$.
[doi:10.1017/S0885715621000580]

Key words: powder diffraction, Rietveld refinement, leucite minerals, silicate framework structures

I. INTRODUCTION

Synthetic anhydrous analogues of the silicate framework minerals leucite ($KAlSi_2O_6$) and pollucite ($CsAlSi_2O_6$) can be prepared with the general formulae $A_2BSi_5O_{12}$ and $ACSi_2O_6$; where A is a monovalent alkali metal cation, B is a divalent cation, and C is a trivalent cation. These structures all have the same topology with B and C cations partially substituting onto tetrahedrally coordinated sites (T-sites) in the silicate framework and charge balancing A cations sitting in extra-framework channels. The A cations can be replaced by ion exchange, Cs containing silicate framework minerals are of potential technological interest as storage media for radioactive Cs from nuclear waste (Gatta *et al.*, 2008).

We have used X-ray and neutron powder diffraction to determine and Rietveld refine the ambient temperature crystal structures of leucite analogues with the general formulae $A_2BSi_5O_{12}$ and $ACSi_2O_6$. Crystal structures have been refined in the $Ia\bar{3}d$ cubic and $I4_1/a$ tetragonal space groups (A = K, Rb, Cs; B = Mg, Mn, Co, Cu, Zn; C = Fe^{3+}, Ga; Bell and Henderson, 1994a, 1994b, 2018, 2020; Bell *et al.,* 1994a, 2010). These structures all have *disordered* T-site cations and also have A cation sites fully occupied with either K, Rb, or Cs. Crystal structures have also been refined at ambient temperature for $P2_1/c$ monoclinic crystal structures of leucite analogues with the general formulae $A_2BSi_5O_{12}$ (A = K, B = Mg, Fe^{2+}, Co, Zn; Bell *et al.,* 1994a; Bell and Henderson, 2018) and also for *Pbca* orthorhombic (A = Rb; B = Mg, Mn, Ni, Cd; Bell and Henderson, 1996, 2009, 2016) and (A = Cs; B = Mg, Mn, Co, Ni, Cu, Zn, Cd; Bell *et al.*, 1994b, 2010; Bell and Henderson, 1996, 2009). These structures all have *ordered* T-site cations and also have A cation sites fully occupied with either K, Rb, or Cs. $Cs_2ZnSi_5O_{12}$ undergoes a reversible phase transition from *Pbca* to $Pa\bar{3}$ on heating to 566 K (Bell and Henderson, 2012). $K_2MgSi_5O_{12}$ and $K_2ZnSi_5O_{12}$ both undergo phase transitions from $P2_1/c$ to *Pbca* on heating to 622 K ($K_2MgSi_5O_{12}$; Redfern and Henderson, 1996) and over the temperature range 843–868 K ($K_2ZnSi_5O_{12}$; Bell *et al.*, 2021). $KGaSi_2O_6$ undergoes a phase transition from $I4_1/a$ to $Ia\bar{3}d$ over the temperature range 673–970 K (Bell and Henderson, 2020). $Cs_2X^{2+}Si_5O_{12}$ (X = Cd, Cu, Zn) all retain the cation ordered *Pbca* orthorhombic structure below 10 K (Bell, 2021).

$RbCsX^{2+}Si_5O_{12}$ (X = Mg, Ni, Cd) leucite analogues, with two different extra-framework alkali metal cations, all have the *Pbca* structure with ordered T-site cations (Bell and Henderson, 2019). For X = Ni and Cd, these structures have disordered extra-framework cations, but, for X = Mg, there is partial extra-framework cation ordering.

In this paper, we report the Rietveld refinements (Rietveld, 1969) of three more T-site cation-disordered synthetic leucite analogues with stoichiometries of $Cs_2NiSi_5O_{12}$, $RbGaSi_2O_6$, and $CsGaSi_2O_6$.

II. EXPERIMENTAL

A. Sample synthesis

All three samples were prepared from appropriate stoichiometric mixtures of Rb_2CO_3, Cs_2CO_3, SiO_2, NiO, and Ga_2O_3. The starting mixture for $Cs_2NiSi_5O_{12}$ was loaded into a platinum crucible and heated for 24 h at 873 K to decompose the carbonate. The mixture was then heated at 1673 K for 90 min before quenching by dipping the base of the crucible in water. The resultant glass was then reground and heated at 1393 K for 5 days; this produced a dark blue

[a]Author to whom correspondence should be addressed. Electronic mail: anthony.bell@shu.ac.uk

powdered sample. The starting mixtures for $RbGaSi_2O_6$ and $CsGaSi_2O_6$ were also loaded into platinum crucibles. Both mixtures were heated at 10 K min^{-1} from room temperature to 873 K; the temperature was then maintained at 873 K for 12 h, in order to decompose carbonates. The mixtures were then heated to 1473 K at 10 K min^{-1} and the temperature was then maintained at 1473 K for 10 h. Each crucible was removed from the furnace and quenched by dipping the base of the crucible in water. The resultant glasses were then reground and heated up at 1473 K for 7 days before cooling at 2 K min^{-1} to room temperature. This produced white powdered samples.

B. X-ray powder diffraction data collection

After heating the samples were removed from the metal capsules, ground with a mortar and pestle and then mounted on low-background silicon wafers with a drop of acetone prior to ambient temperature X-ray powder diffraction (XRD).

For $Cs_2NiSi_5O_{12}$, data were collected on a PANalytical Empyrean diffractometer using Co$K\alpha$ X-rays with an iron β-filter and a 3.3473° 2θ wide 255 channel PIXCEL-3D area detector. Data were collected in a single scan over 66 h using Data Collector 5.1a (PANalytical, 2014). These data were collected over the range 12–140° 2θ with a step width of 0.0131° 2θ and an effective counting time of 5998 s per point, the beam size was defined with a 20 mm mask, fixed divergence antiscatter (¼°) slit and automatic divergence slit with a 15-mm long beam footprint. These diffracted intensities were converted from the automatic divergence slit mode to the fixed divergence slit mode in HighScore Plus (PANalytical, 2009) prior to data analysis.

For the $RbGaSi_2O_6$ and $CsGaSi_2O_6$ samples, data were collected on a PANalytical X'Pert Pro MPD using Cu$K\alpha$ X-rays, with a nickel β-filter and a 3.3473° 2θ wide 255 channel PIXCEL-1D area detector. These data were collected over the range 8–100° 2θ with a step width of 0.0131° 2θ using Data Collector 5.5a (PANalytical, 2017). The beam size was defined with a 20 mm mask, fixed antiscatter (¼°) and divergence (⅛°) slits. For $RbGaSi_2O_6$, a single-scan was collected lasting 33 h and an effective counting time of 4175 s per point. For $CsGaSi_2O_6$, a single-scan was collected lasting 24 h and an effective counting time of 3035 s per point.

No smoothing or α_2 stripping was done on any of these data. Both diffractometers were calibrated with an external NIST 640e silicon standard.

C. XRD data analysis

All powder diffraction data were using HighScore Plus and the ICDD Powder Diffraction File. Analysis of the powder diffraction data for $Cs_2NiSi_5O_{12}$ showed that this sample was single-phase cubic and the position of the Bragg reflections in the powder diffraction data matched the cubic pattern PDF# 00-037-0335 for $Cs_2NiSi_5O_{12}$. However, analysis of the powder diffraction data for $RbGaSi_2O_6$ showed that this sample consisted of two phases. The main phase was $I4_1/a$ tetragonal $RbGaSi_2O_6$ PDF# 00-037-0350 with $C2/m$ monoclinic Ga_2O_3 PDF# 00-043-1012 as a minor phase. A similar analysis of $CsGaSi_2O_6$ also showed $I\bar{4}3d$ cubic pattern PDF# 00-050-0175 for $CsGaSi_2O_6$ as the main phase and $C2/m$ monoclinic Ga_2O_3 PDF# 00-043-1012 as a minor phase.

Rietveld refinements were done using FULLPROF (Rodríguez-Carvajal, 1993). Backgrounds were fitted by linear interpolation between a set of background points with refinable heights. The Thompson-Cox-Hastings Pseudo-Voigt function (van Laar and Yelon, 1984), convoluted with asymmetry due to axial divergence (Finger *et al.*, 1994), was used to model the profile shape.

The crystal structure of $Cs_2NiSi_5O_{12}$ was refined using the $Ia\bar{3}d$ cubic structure of $Cs_2CuSi_5O_{12}$ (Bell *et al.*, 2010) as the starting model. In this starting model, Ni replaced Cu on the disordered T-site. In this crystal structure, there is one $Ia\bar{3}d$ 16b Wyckoff special position site which is 100% occupied by Cs, there is one 48 g special position site which is 1/6th occupied by Ni and 5/6th by Si (T-site occupancies were not refined) and there is a 96 h general position 100% occupied by O. A stoichiometry of $Cs_2NiSi_5O_{12}$ was assumed. The isotropic temperature factors of the T-site atoms Si and Ni were constrained to be the same. It should be noted that one of the authors (AMTB) published a *Pbca* orthorhombic structure for $Cs_2NiSi_5O_{12}$, with ordered T-site cations and *a*, *b*, and *c* being very close but slightly different (Bell and Henderson, 1996). However, the XRD data for this sample did not show the slight orthorhombic distortion that was seen in the synchrotron XRD data used for the earlier structure refinement.

The crystal structure of $RbGaSi_2O_6$ was refined using the $I4_1/a$ structure of $KGaSi_2O_6$ (Bell and Henderson, 2020) as the starting model with Rb replacing K on the extra-framework cation site. In this crystal structure, all atoms were located on the $I4_1/a$ 16f Wyckoff general position. There is one 16f position for Rb, three 16*f* positions for T-sites (disordered 1/3rd Ga and 2/3rd Si, T-site occupancies were not refined), and six 16*f* positions for O. The isotropic temperature factors of the T-site atoms Si and Ga were constrained to be the same on each T-site but were allowed to vary between different T-sites. All isotropic temperature factors for the six O sites were constrained to have the same value. As was done for $KGaSi_2O_6$ the T–O interatomic distances were soft constrained to be 1.68 ± 0.02 Å (the average bond distance for tetrahedral Si–O and Ga–O) assuming complete T-site disorder (1/3Ga:2/3Si on each T-site) as it was not possible to refine chemically sensible T-site occupancies. Rietveld refinements in noncubic leucite structures without soft interatomic distance constraints tend to give unrealistic interatomic T–O distances.

The crystal structure of $CsGaSi_2O_6$ was refined using the $I\bar{4}3d$ cubic structure of $RbBSi_2O_6$ (Filatov *et al.*, 2011) as the starting model. This matched the space group assignment of the $CsGaSi_2O_6$ PDF# 00-050-0175. In this starting model, Ga replaced B on the disordered T-site, which is occupied by 1/3rd Ga and 2/3rd Si (T-site occupancies were not refined), and Cs replaced Rb on the extra-framework cation site. In this crystal structure, there is one $I\bar{4}3d$ 16c Wyckoff special position site which is 100% occupied by Cs. There are also three $I\bar{4}3d$ 48e Wyckoff general position sites, one of these is occupied by the disordered Ga/Si T-site and two are 100% occupied by O. The Rietveld refinements for $RbGaSi_2O_6$ and $CsGaSi_2O_6$ both used the crystal structure of Ga_2O_3 (da Silva *et al.*, 2012) to fit the minor phase. The $RbGaSi_2O_6$ sample contained 11.8(1) wt.% Ga_2O_3 and the $CsGaSi_2O_6$ sample contained 9.2(1) wt.% Ga_2O_3.

TABLE I. Refined lattice parameters compared with those for starting structures

Stoichiometry	Space group	a (Å)	b (Å)	c (Å)	V (Å^3)
$Cs_2NiSi_5O_{12}$	$Ia\bar{3}d$	13.64694(9)	13.64694(9)	13.64694(9)	2541.59(3)
$Cs_2CuSi_5O_{12}$	$Ia\bar{3}d$	13.6322(4)	13.6322(4)	13.6322(4)	2533.4(2)
$RbGaSi_2O_6$	$I4_1/a$	13.3703(2)	13.3703(2)	13.7983(2)	2466.66(7)
$KGaSi_2O_6$	$I4_1/a$	13.1099(4)	13.1099(4)	13.8100(4)	2373.50(12)
$CsGaSi_2O_6$	$I\bar{4}3d$	13.72124(8)	13.72124(8)	13.72124(8)	2583.33(2)
$RbBSi_2O_6$	$I\bar{4}3d$	12.7898(1)	12.7898(1)	12.7898(1)	2092.14(5)

TABLE II. Refined interatomic distances, $Ia\bar{3}d$ cubic structures

	A–O x6 (Å)	A–O x6 (Å)	T–O x2 (Å)	T–O x2 (Å)
$Cs_2NiSi_5O_{12}$	3.547(4)	3.357(4)	1.629(4)	1.655(4)
$Cs_2CuSi_5O_{12}$	3.528(5)	3.363(5)	1.631(4)	1.652(5)

TABLE III. Refined interatomic angles, $Ia\bar{3}d$ cubic structures

	O–T–O x2 (°)	O–T–O x2 (°)	O–T–O (°)	O–T–O (°)	T–O–T (°)
$Cs_2NiSi_5O_{12}$	113.0(4)	111.9(3)	105.0(3)	102.3(4)	143.3(2)
$Cs_2CuSi_5O_{12}$	112.6(3)	112.0(3)	106.4(4)	101.3(4)	142.9(3)

VESTA (Momma and Izumi, 2011) was used to plot crystal structures.

III. RESULTS AND DISCUSSION

Crystal structures have been refined for $Cs_2NiSi_5O_{12}$, $RbGaSi_2O_6$, and $CsGaSi_2O_6$ leucite analogues from XRD data. All refined structures have disordered T-site cations. $Cs_2NiSi_5O_{12}$ is isostructural with $Ia\bar{3}d$ cubic $Cs_2CuSi_5O_{12}$; $RbGaSi_2O_6$ is isostructural with $I4_1/a$ tetragonal $KGaSi_2O_6$; and $CsGaSi_2O_6$ is isostructural with $I\bar{4}3d$ cubic $RbBSi_2O_6$. Table I shows the comparison of the refined lattice parameters for $Cs_2NiSi_5O_{12}$, $RbGaSi_2O_6$, and $CsGaSi_2O_6$ with the $Cs_2CuSi_5O_{12}$ (Bell *et al.*, 2010), $KGaSi_2O_6$ (Bell and Henderson, 2020), and $RbBSi_2O_6$ (Filatov *et al.*, 2011) starting structures used for Rietveld refinement. Tables II–VII similarly show refined interatomic distances and angles; the mean T–O distances are close to the constraint distances, the mean O–T–O angles are close to the ideal tetrahedral angle of 109.47°. Table VIII similarly shows the tetrahedral angle variances for the T-sites (Robinson *et al.*, 1971) in the silicate framework structures.

A. $Cs_2NiSi_5O_{12}$ structure

Figures 1 and 2 respectively show the Rietveld difference and the VESTA crystal structure plots for the refined crystal structure of $Cs_2NiSi_5O_{12}$. Table I shows that this crystal structure has a unit cell volume that is slightly larger than the isostructural $Cs_2CuSi_5O_{12}$ which was used as a starting model for Rietveld refinement. However, the ionic radius (Shannon, 1976) for Ni^{2+} (0.69 Å) is smaller than that for Cu^{2+} (0.71 Å), it would be expected that the smaller ionic radius for Ni^{2+} would result in a smaller unit cell compared with that for $Cs_2CuSi_5O_{12}$. This discrepancy may be due to $Cs_2NiSi_5O_{12}$ not having the assumed stoichiometry. Table II shows that one set of Cs–O distances is slightly larger for $Cs_2NiSi_5O_{12}$ compared with $Cs_2CuSi_5O_{12}$. However, the other set of Cs–O distances are equivalent between error limits. Table II also shows that both sets of T–O distances are equivalent between error limits for $Cs_2NiSi_5O_{12}$ and $Cs_2CuSi_5O_{12}$. Table III shows that two of the six O–T–O angles are different between error limits for $Cs_2NiSi_5O_{12}$ and $Cs_2CuSi_5O_{12}$, but the T–O–T angles are equivalent between error limits for $Cs_2NiSi_5O_{12}$ and $Cs_2CuSi_5O_{12}$. Table VIII shows that tetrahedral distortions for $Cs_2NiSi_5O_{12}$ and $Cs_2CuSi_5O_{12}$ are very close.

B. $RbGaSi_2O_6$ structure

Figures 3 and 4 respectively show the Rietveld difference and the VESTA crystal structure plots for the refined crystal structure of $RbGaSi_2O_6$. Note that Figure 4 shows that this tetragonal crystal structure has a slightly collapsed silicate

TABLE IV. Refined interatomic distances (Å)

		A = K	A = Rb
A	O1	3.51(3)	3.21(2)
A	O1	3.24(3)	3.20(2)
A	O2	3.92(3)	3.43(2)
A	O2	3.38(3)	3.34(1)
A	O3	3.33(3)	3.34(2)
A	O3	3.17(3)	3.66(1)
A	O4	2.87(3)	3.20(1)
A	O4	3.90(3)	3.60(1)
A	O5	2.93(3)	3.18(2)
A	O5	3.39(3)	3.98(1)
A	O6	3.44(2)	3.65(2)
A	O6	3.41(3)	3.28(2)
mean A–O		3.374(29)	3.423(15)
T1	O1	1.63(2)	1.72(2)
T1	O1	1.61(2)	1.62(2)
T1	O2	1.63(2)	1.76(2)
T1	O4	1.58(2)	1.59(1)
T2	O2	1.73(2)	1.64(2)
T2	O3	1.65(2)	1.79(1)
T2	O4	1.60(2)	1.54(1)
T2	O5	1.73(2)	1.62(1)
T3	O3	1.66(2)	1.64(1)
T3	O5	1.70(2)	1.68(1)
T3	O6	1.60(2)	1.53(2)
T3	O6	1.66(2)	1.76(2)
mean T1–O		1.648(20)	1.658(14)
mean T2–O		1.614(19)	1.672(15)
mean T3–O		1.677(20)	1.649(14)
mean T–O		1.655(20)	1.654(15)

$I4_1/a$ tetragonal structures. $AGaSi_2O_6$ (A = K, Rb). T = disordered Si/Ga.

TABLE V. Refined interatomic angles (°)

			A = K	A = Rb
O1	T1	O1	107.0(2.0)	118.5(1.5)
O1	T1	O2	96.6(1.7)	89.8(1.1)
O1	T1	O4	132.0(2.0)	118.4(1.4)
O1	T1	O2	124.0(2.0)	107.8(1.5)
O1	T1	O4	99.0(2.0)	105.6(1.4)
O2	T1	O4	101.5(1.8)	116.0(1.2)
O2	T2	O3	105.2(1.9)	113.9(1.2)
O2	T2	O4	125.0(2.0)	109.6(1.2)
O2	T2	O5	101.4(1.8)	111.3(1.4)
O3	T2	O4	117.9(1.7)	108.5(1.1)
O3	T2	O5	87.5(1.7)	107.3(1.2)
O4	T2	O5	113.0(2.0)	106.0(1.2)
O3	T3	O5	105.1(1.9)	97.5(1.2)
O3	T3	O6	97.2(1.8)	108.8(1.4)
O3	T3	O6	133.0(2.0)	113.9(1.3)
O5	T3	O6	106.5(1.6)	110.0(1.2)
O5	T3	O6	99.1(1.8)	106.1(1.3)
O6	T3	O6	114.1(1.9)	118.4(1.4)
mean O–T–O			109.17(1.88)	109.30(1.29)
mean O–T1–O			110.02(1.93)	109.35(1.35)
mean O–T2–O			108.33(1.87)	109.43(1.22)
mean O–T3–O			109.17(1.85)	109.12(1.30)
T1	O1	T1	135.2(1.3)	131.8(9)
T1	O2	T2	168.9(1.4)	143.3(9)
T2	O3	T3	135.2(1.3)	142.4(8)
T1	O4	T2	144.4(1.4)	148.1(9)
T2	O5	T3	123.6(1.3)	141.1(9)
T3	O6	T3	142.4(1.4)	131.8(9)
mean T–O–T			141.62(1.36)	139.75(89)

$I4_1/a$ tetragonal structures. AGaSi$_2$O$_6$ (A = K, Rb). T = disordered Si/Ga.

framework structure compared with the cubic structure in Figure 2. Table I shows that the crystal structure of RbGaSi$_2$O$_6$ has a larger unit cell volume than that of KGaSi$_2$O$_6$ which was used as a starting model for Rietveld refinement, this reflects the difference in the ionic radii for Rb^+ (1.72 Å) and K^+ (1.64 Å) cations (Shannon, 1976). However, the ambient temperature c/a ratio for RbGaSi$_2$O$_6$ is 1.032, which is smaller than the ambient temperature c/a ratio for KGaSi$_2$O$_6$, which is 1.053. When KGaSi$_2$O$_6$ is heated the c/a ratio decreases before a phase transition from $I4_1/a$ to $Ia\bar{3}d$ over the temperature range 673–970 K (Bell and Henderson, 2020). It would be interesting to do a high-temperature XRD experiment on RbGaSi$_2$O$_6$ as this smaller c/a ratio would suggest that this leucite analogue would undergo a phase transition from $I4_1/a$ to $Ia\bar{3}d$ at a lower temperature than KGaSi$_2$O$_6$. Table IV shows larger A–O distances for A = Rb compared with A = K, also reflecting the ionic radii difference. The mean T–O distances for RbGaSi$_2$O$_6$ and KGaSi$_2$O$_6$ are the same within error limits. Table IV shows that the mean O–T–O and T–O–T angles for RbGaSi$_2$O$_6$ and KGaSi$_2$O$_6$ are the same within error limits. Table VIII shows that mean tetrahedral distortion for KGaSi$_2$O$_6$ is larger than that for RbGaSi$_2$O$_6$, this reflects the greater collapse (Taylor and Henderson, 1968) of the silicate framework structure with the smaller K^+ cation compared with the larger Rb^+ cation.

TABLE VI. Refined interatomic distances (Å)

	CsGaSi$_2$O$_6$	RbBSi$_2$O$_6$
A1–O1 x3	3.450(9)	3.299(7)
A1–O1 x3	3.648(9)	3.456(8)
A1–O2 x3	3.106(9)	2.917(7)
A1–O2 x3	3.651(9)	3.400(8)
mean A–O	3.464(9)	3.268(8)
T1–O1	1.653(12)	1.522(8)
T1–O1	1.635(10)	1.596(9)
T1–O2	1.691(10)	1.517(8)
T1–O2	1.754(11)	1.629(9)
mean T–O	1.683(11)	1.566(8)

$I\bar{4}3d$ cubic structures. A = Cs/Rb, T = disordered Si/Ga and Si/B.

TABLE VII. Refined interatomic angles (°)

			CsGaSi$_2$O$_6$	RbBSi$_2$O$_6$
O1	T1	O1	119.1(9)	111.8(6)
O1	T1	O2	110.0(9)	106.9(5)
O1	T1	O2	100.6(9)	104.7(5)
O1	T1	O2	103.9(8)	113.7(6)
O1	T1	O2	112.7(8)	105.1(5)
O2	T1	O2	110.7(8)	114.5(6)
mean O–T–O			109.5(9)	109.5(5)
T1	O1	T1	142.0(1.1)	128.9(6)
T2	O1	T2	133.2(7)	150.2(7)
mean T–O–T			137.6(9)	139.6(6)

$I\bar{4}3d$ cubic structures. A = Cs/Rb, T = disordered Si/Ga and Si/B

C. CsGaSi$_2$O$_6$ structure

Figures 5 and 6 respectively show the Rietveld difference and the VESTA crystal structure plots for the refined crystal structure of CsGaSi$_2$O$_6$. Table I shows that the crystal structure of CsGaSi$_2$O$_6$ has a larger a unit-cell volume than that of RbBSi$_2$O$_6$ which was used as a starting model for Rietveld refinement, this reflects the differences in the ionic radii for Cs^+ (2.02 Å), Ga^{3+} (0.61 Å), Rb^+ (1.86 Å), and B^{3+} (0.25 Å) cations (Shannon, 1976). CsGaSi$_2$O$_6$ has the $I\bar{4}3d$ cubic crystal structure, unlike RbGaSi$_2$O$_6$, which has the $I4_1/a$ tetragonal structure. These differences in cation size mean that the silicate framework for the RbGaSi$_2$O$_6$ is more collapsed (Taylor and Henderson, 1968) than for CsGaSi$_2$O$_6$, and consequently, there is a lowering of symmetry for the crystal structure. Table VI shows that for CsGaSi$_2$O$_6$ the A–O and T–O distances are larger than those for the RbBSi$_2$O$_6$ due to the differences in ionic radii for the cations present in these crystal structures. Table VII shows that three of the six O–T–O angles are

TABLE VIII. Tetrahedral angle variance [σ^2, deg^2]: $\sigma^2 = \Sigma(\theta - 109.47)^2/5$ (Robinson *et al.*, 1971), where θ is the O–T–O tetrahedral angle.

Stoichiometry	Space group	σ^2 (T1) deg	σ^2 (T2) deg	σ^2 (T3) deg	σ^2 (T) deg^2
Cs$_2$NiSi$_5$O$_{12}$	$Ia\bar{3}d$				21.62
Cs$_2$CuSi$_5$O$_{12}$	$Ia\bar{3}d$				21.71
RbGaSi$_2$O$_6$	$I4_1/a$	121.72	8.14	50.95	60.27(57.36)
KGaSi$_2$O$_6$	$I4_1/a$	212.72	178.15	172.22	187.70(21.87)
CsGaSi$_2$O$_6$	$I\bar{4}3d$				42.93
RbBSi$_2$O$_6$	$I\bar{4}3d$				19.42

Mean variance and standard deviation is given for the three tetrahedral sites in each $I4_1/a$ structure. Variance is given for the single tetrahedral site in each $Ia\bar{3}d$ and $I\bar{4}3d$ structure.

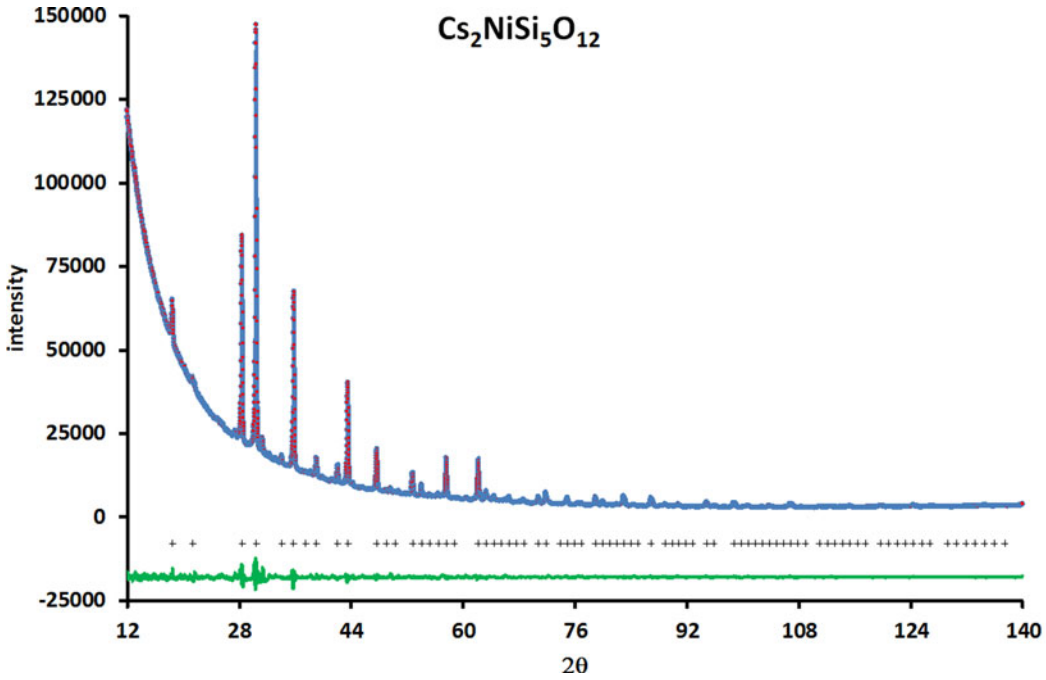

Figure 1. Rietveld difference plot for $Cs_2NiSi_5O_{12}$. Red circles represent observed data points, the blue line represents calculated data points, the green line represents difference curve, and black crosses represent positions of Bragg reflections. *R*-factors for this refinement were: $R_p = 21.5314\%$, $R_{wp} = 11.5115\%$, $R_{exp} = 4.7035\%$, $\chi^2 = 6.2111$.

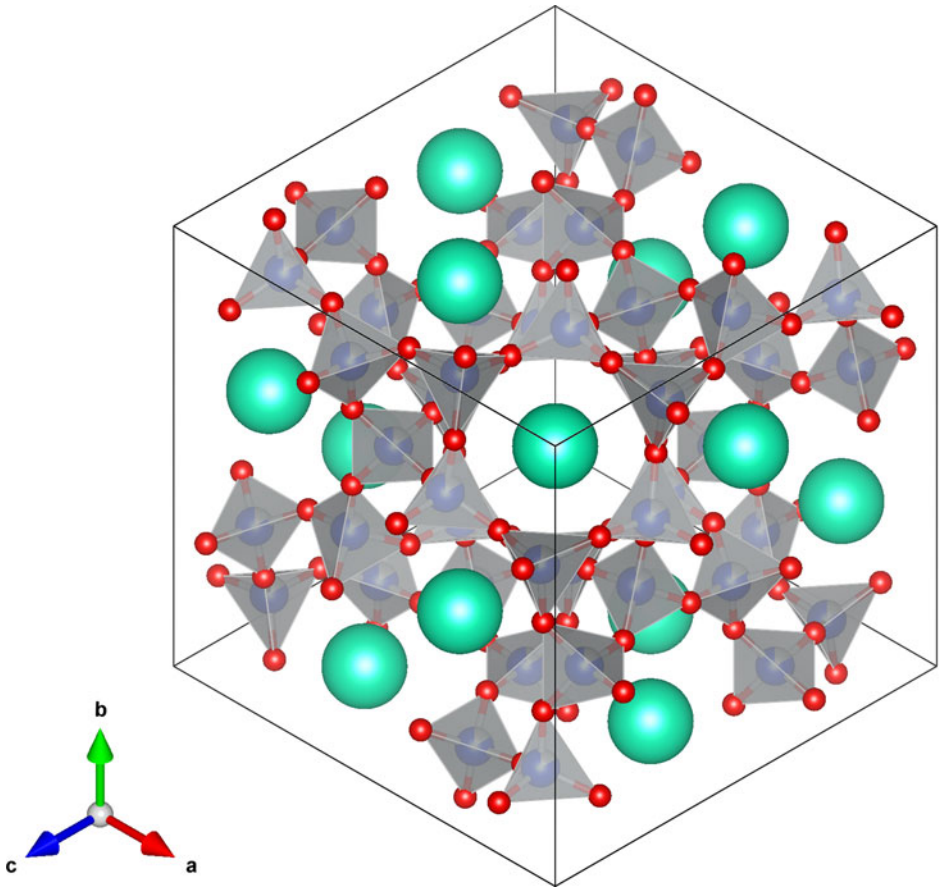

Figure 2. VESTA $Ia\bar{3}d$ cubic structure plot for $Cs_2Ni^{2+}Si_5O_{12}$, viewed down [111] showing a channel for extra-framework light blue Cs^+ cations. Disordered (Si/Ni)O_4 tetrahedra are shown in gray with O^{2-} anions are shown in red.

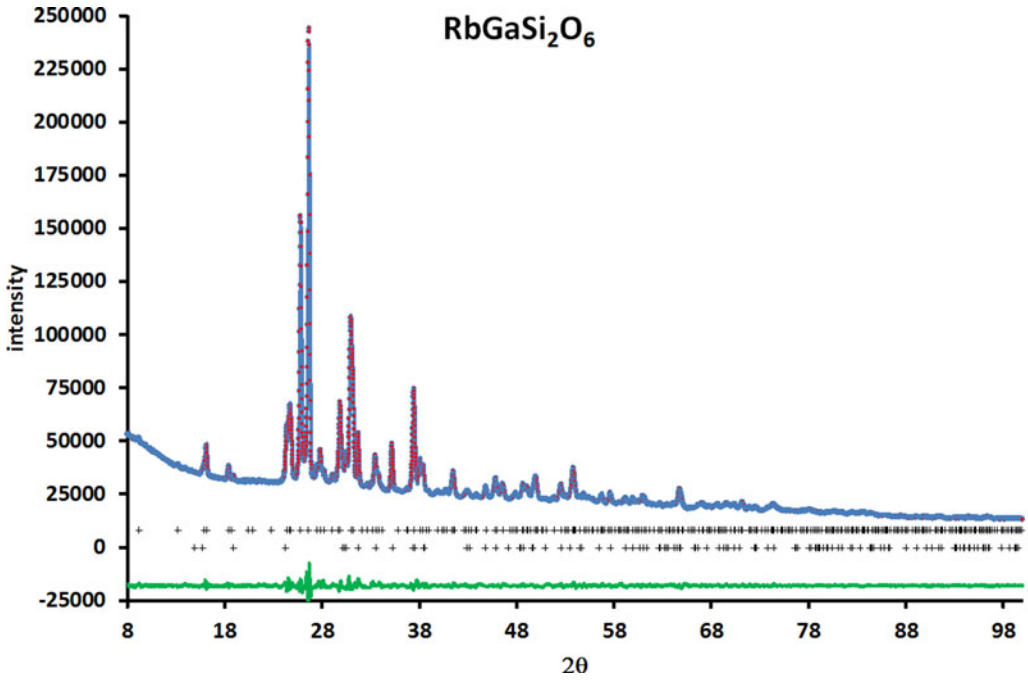

Figure 3. Rietveld difference plot for $RbGaSi_2O_6$. Red circles represent observed data points, the blue line represents calculated data points, and the green line represents difference curve. The upper line of black crosses represent positions of Bragg reflections for $RbGaSi_2O_6$ and the lower line of black crosses represent positions of Bragg reflections for Ga_2O_3 impurity. *R*-factors for this refinement were: $R_p = 10.1855\%$, $R_{wp} = 8.2308\%$, $R_{exp} = 2.7240\%$, $\chi^2 = 9.2667$.

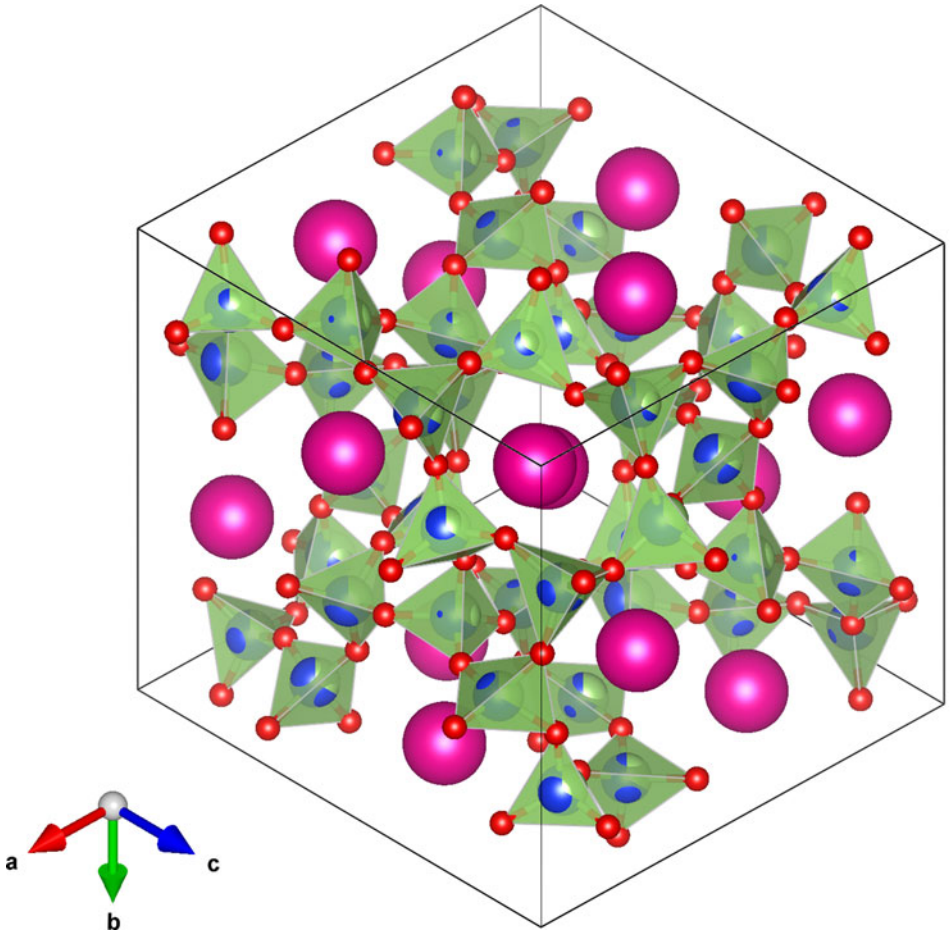

Figure 4. VESTA $I4_1/a$ tetragonal structure plot for $RbGaSi_2O_6$, viewed down [1–11] showing a channel for extra-framework pink Rb^+ cations. Disordered (Si/Ga)O_4 tetrahedra are shown in light green with O^{2-} anions are shown in red.

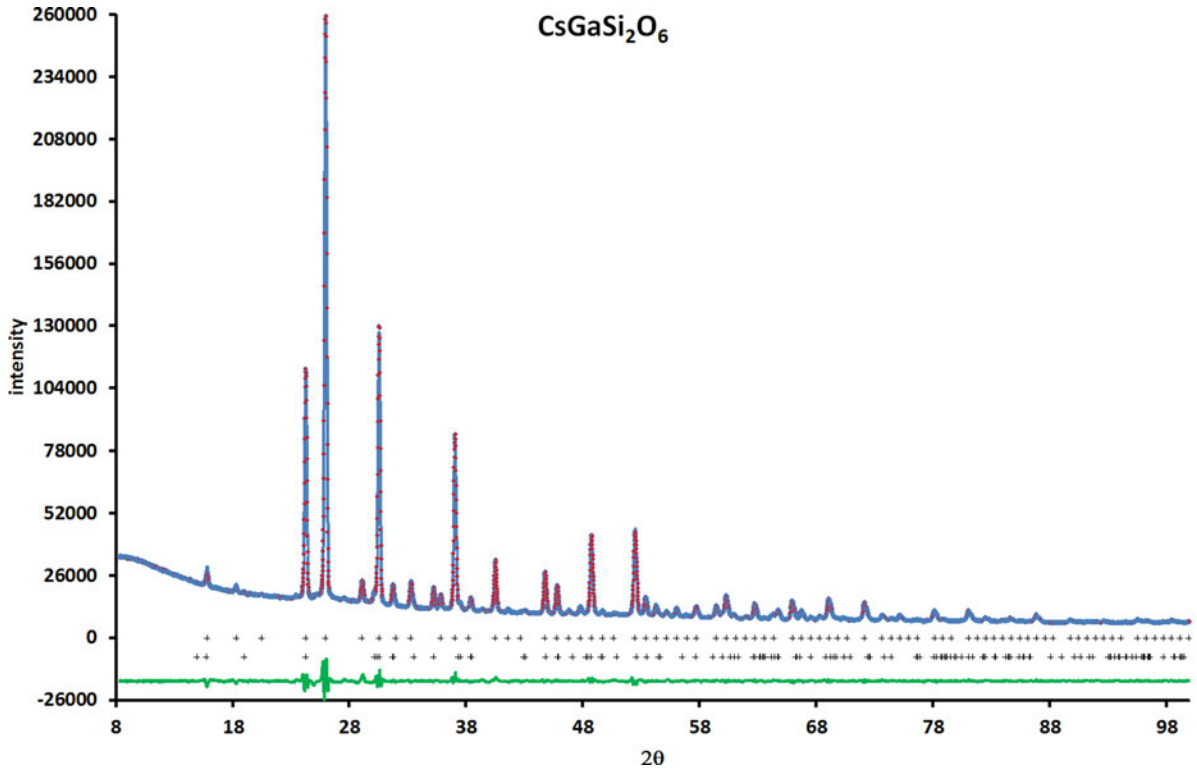

Figure 5. Rietveld difference plot for $CsGaSi_2O_6$. Red circles represent observed data points, the blue line represents calculated data points, and the green line represents difference curve. The upper line of black crosses represent positions of Bragg reflections for $CsGaSi_2O_6$ and the lower line of black crosses represent positions of Bragg reflections for Ga_2O_3 impurity. *R*-factors for this refinement were: $R_p = 9.9377\%$, $R_{wp} = 8.0887\%$, $R_{exp} = 2.5680\%$, $\chi^2 = 10.4871$.

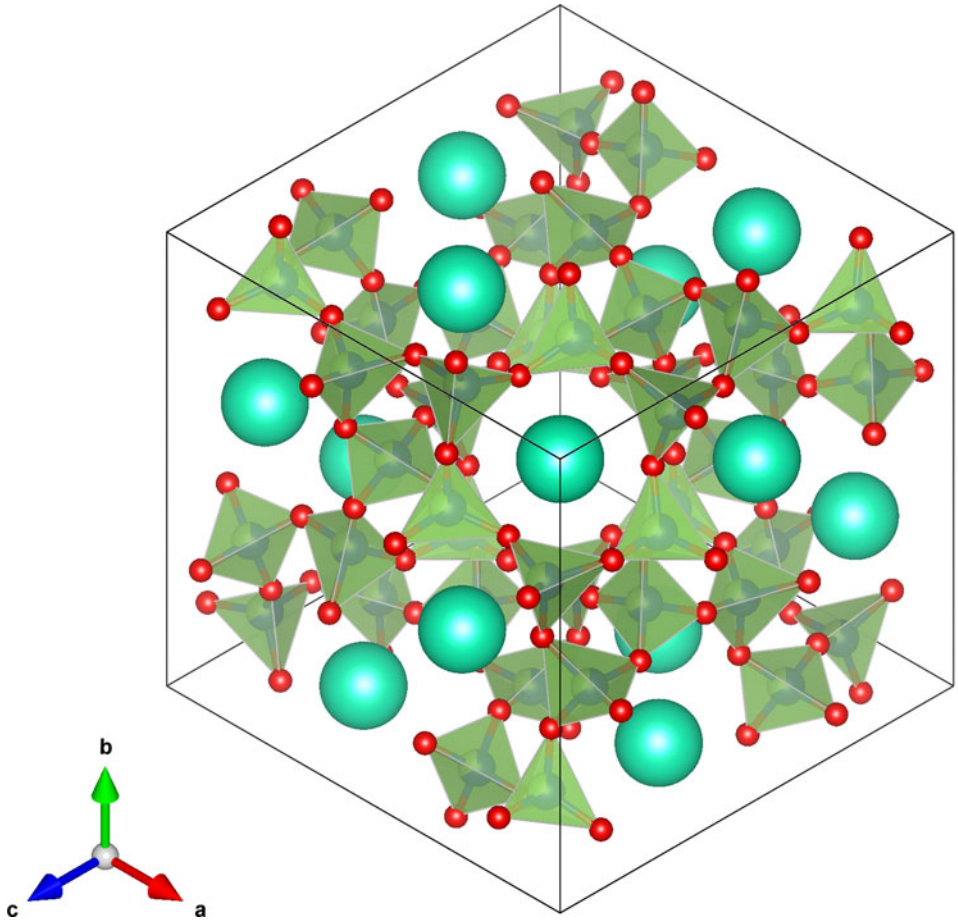

Figure 6. VESTA $I\bar{4}3d$ cubic structure plot for $CsGaSi_2O_6$, viewed down [111] showing a channel for extra-framework light blue Cs^+ cations. Disordered (Si/Ga)O_4 tetrahedra are shown in light green with O^{2-} anions are shown in red.

different between error limits for $CsGaSi_2O_6$ and $RbBSi_2O_6$. The mean T–O–T angles for $CsGaSi_2O_6$ are smaller than those for $RbBSi_2O_6$, reflecting the greater framework collapse of $RbBSi_2O_6$ compared with $CsGaSi_2O_6$. Table VIII shows that tetrahedral distortion for $CsGaSi_2O_6$ is larger than that for $RbBSi_2O_6$. This reflects the greater distortion of the silicate framework structure by incorporation of the larger Ga^{3+} cation into the framework compared with the smaller B^{3+} cation.

The *R*-factors for this refinement of the $CsGaSi_2O_6$ crystal structure in $I\bar{4}3d$ were: $R_p = 9.9377\%$, $R_{wp} = 8.0887\%$, $R_{exp} = 2.5680\%$, $\chi^2 = 10.4871$. However, it should be noted that a refinement of the $CsGaSi_2O_6$ crystal structure in $Ia\bar{3}d$, using the cubic structure of $CsAlSi_2O_6$ (Yanase *et al.*, 1997) as a starting structure, gave the following *R*-factors: $R_p = 10.3604\%$, $R_{wp} = 8.4084\%$, $R_{exp} = 2.5708\%$, $\chi^2 = 11.5234$. These *R*-factors are only slightly worse than those for $I\bar{4}3d$, suggesting that the crystal structures in these two different space groups show some similarities. $Ia\bar{3}d$ is a supergroup of $I\bar{4}3d$, it would also be interesting to try a high-temperature XRD experiment on $CsGaSi_2O_6$ to see if there might be a phase transition from $I\bar{4}3d$ to $Ia\bar{3}d$.

IV. CONCLUSIONS

Crystal structures have been refined for $Cs_2NiSi_5O_{12}$, $RbGaSi_2O_6$, and $CsGaSi_2O_6$ synthetic leucite analogues. All refined structures have disordered T-site cations. $Cs_2NiSi_5O_{12}$ is isostructural with $Ia\bar{3}d$ cubic $Cs_2CuSi_5O_{12}$; $RbGaSi_2O_6$ is isostructural with $I4_1/a$ tetragonal $KGaSi_2O_6$, and $CsGaSi_2O_6$ is isostructural with $I\bar{4}3d$ cubic $RbBSi_2O_6$.

V. DEPOSITED DATA

CIF files with information related to crystal structure, interatomic distances, and angles, and powder diffraction data for $Cs_2NiSi_5O_{12}$, $RbGaSi_2O_6$, and $CsGaSi_2O_6$ synthetic leucite analogues were deposited with the ICDD. You may request these data from ICDD at info@icdd.com.

ACKNOWLEDGEMENTS

We wish to acknowledge the use of the EPSRC funded National Chemical Database Service hosted by the Royal Society of Chemistry. We also wish to thank Ms Mirjam Skof of Sheffield Hallam University for her assistance with the use of a glove box.

Bell, A. M. T. (**2021**). "Rietveld refinement of the low temperature crystal structures of $Cs_2XSi_5O_{12}$ (X = Cu, Cd and Zn)," Eur. J. Chem. **12**(1), 60–63.

Bell, A. M. T. and Henderson, C. M. B. (**1994a**). "Rietveld refinement of dry-synthesized $Rb_2ZnSi_5O_{12}$ leucite by synchrotron X-ray powder diffraction," Acta Crystallogr. **C50**, 984–986.

Bell, A. M. T. and Henderson, C. M. B. (**1994b**). "Rietveld refinement of the structures of dry-synthesized *M* Fe(III) Si_2O_6 leucites (M=K,Rb,Cs) by synchrotron X-ray powder diffraction," Acta Crystallogr. **C50**, 1531–1536.

Bell, A. M. T. and Henderson, C. M. B. (**1996**). "Rietveld refinement of the orthorhombic *Pbca* structures of $Rb_2CdSi_5O_{12}$, $Cs_2MnSi_5O_{12}$, $Cs_2CoSi_5O_{12}$ and $Cs_2NiSi_5O_{12}$ leucites by synchrotron X-ray powder diffraction," Acta Crystallogr. **C52**, 2132–2139.

Bell, A. M. T. and Henderson, C. M. B. (**2009**). "Crystal structures and cation ordering in $Cs_2MgSi_5O_{12}$, $Rb_2MgSi_5O_{12}$ and $Cs_2ZnSi_5O_{12}$ leucites," Acta Crystallogr. **B65**, 435–444.

Bell, A. M. T. and Henderson, C. M. B. (**2012**). "High-temperature synchrotron X-ray powder diffraction study of $Cs_2XSi_5O_{12}$ (X=Cd, Cu, Zn) leucites," Mineral. Mag. **76**(5), 1257–1280.

Bell, A. M. T. and Henderson, C. M. B. (**2016**). "Rietveld refinement of the crystal structures of $Rb_2XSi_5O_{12}$ (X=Ni, Mn)," Acta Crystallogr. **E72**, 249–252.

Bell, A. M. T. and Henderson, C. M. B. (**2018**). "Crystal structures of $K_2[XSi_5O_{12}]$ (X=Fe^{2+}, Co, Zn) and $Rb_2[XSi_5O_{12}]$ (X=Mn) leucites: comparison of monoclinic $P2_1/c$ and Ia/d polymorph structures and inverse relationship between tetrahedral cation (T=Si and X)–O bond distances and intertetrahedral T–O–T angles," Acta Crystallogr. **B74**, 274–286.

Bell, A. M. T. and Henderson, C. M. B. (**2019**). "A study of possible extra-framework cation ordering in *Pbca* leucite structures with stoichiometry $RbCsX^{2+}Si_5O_{12}$ (X=Mg, Ni, Cd)," Powder Diffr. **34** (Suppl. S1), S2–S7.

Bell, A. M. T. and Henderson, C. M. B. (**2020**). "Tetragonal-cubic phase transition in $KGasi_2o_6$ synthetic leucite analogue and its probable mechanism," J. Solid State Chem. **284**, 121142.

Bell, A. M. T., Henderson, C. M. B., Redfern, S. A. T., Cernik, R. J., Champness, P. E., Fitch, A. N., and Kohn, S. C. (**1994a**). "Structures of synthetic $K_2MgSi_5O_{12}$ leucites by integrated X-ray powder diffraction, electron diffraction and ^{29}Si MAS NMR methods," Acta Crystallogr. **B50**, 31–41.

Bell, A. M. T., Redfern, S. A. T., Henderson, C. M. B., and Kohn, S. C. (**1994b**). "Structural relations and tetrahedral ordering pattern of synthetic orthorhombic $Cs_2CdSi_5O_{12}$ leucite: a combined synchrotron X-ray powder diffraction and multinuclear MAS NMR study," Acta Crystallogr. **B50**, 560–566.

Bell, A. M. T., Knight, K. S., Henderson, C. M. B., and Fitch, A. N. (**2010**). "Revision of the structure of $Cs_2CuSi_5O_{12}$ leucite as orthorhombic *Pbca*," Acta Crystallogr. **B66**, 51–59.

Bell, A. M. T., Clegg, F., and Henderson, C. M. B. (**2021**). "Monoclinic-orthorhombic first-order phase transition in $K_2ZnSi_5O_{12}$ leucite analogue: transition mechanism and spontaneous strain analysis," Mineral. Mag. (accepted for publication).

da Silva, M. A. F. M., Sosman, L. P., Yokaichiya, F., Mazzocchi, V. L., Parente, C. B. R., Mestnik-Filho, J., Henry, P. F., and Bordallo, H. N. (**2012**). "Neutron powder diffraction measurements of the spinel $MgGa_2O_4$:Cr^{3+} - a comparative study between the high flux diffractometer D2B at the ILL and the high resolution powder diffractometer Aurora at IPEN," J. Phys.: Conf. Ser. **340**, 1–7.

Filatov, S. K., Paufler, P., Georgievskaya, M. I., Levin, A. A., Meyer, D. C., and Bubnova, R. S. (**2011**). "Crystal formation from glass, crystal structure refinement and thermal behavior of $K_{(1-x)}Rb_{(x)}BSi_2O_6$ boroleucite solid solutions from X-ray powder diffraction data," Z. Kristallogr. **226**, 602–612.

Finger, L. W., Cox, D. E., and Jephcoat, A. P. (**1994**). "A correction for powder diffraction peak asymmetry due to axial divergence," J. Appl. Crystallogr. **27**, 892–900.

Gatta, G. D., Rotiroti, N., Fisch, M., Kadiyski, M., and Armbruster, T. (**2008**). "Stability at high-pressure, elastic behaviour and pressure-induced structural evolution of $CsAlSi_5O_{12}$, a potential host for nuclear waste," Phys. Chem. Miner. **35**, 521–533.

Momma, K. and Izumi, F. (**2011**). "VESTA 3 for three-dimensional visualization of crystal, volumetric and morphology data," J. Appl. Crystallogr. **44**, 1272–1276.

PANalytical (**2009**). *High Score Plus 2.2e (Computer Software)* (PANalytical, Almelo, The Netherlands).

PANalytical (**2014**). *Data Collector 5.1a (Computer Software)* (PANalytical, Almelo, The Netherlands).

PANalytical (**2017**). *Data Collector 5.5a (Computer Software)* (PANalytical, Almelo, The Netherlands).

Redfern, S. A. T. and Henderson, C. M. B. (**1996**). "Monoclinic-orthorhombic phase transition in the $K_2MgSi_5O_{12}$ leucite analog," Am. Mineral. **81**, 369–374.

Rietveld, H. M. (**1969**). "A profile refinement method for nuclear and magnetic structures," J. Appl. Crystallogr. **2**, 65–71.

Robinson, K., Gibbs, G. V., and Ribbe, P. H. (**1971**). "Quadratic elongation: a quantitative measure of distortion in coordination polyhedra," Science **172**, 567–570.
Rodríguez-Carvajal, J. (**1993**). "Recent advances in magnetic structure determination by neutron powder diffraction," Physica B **192**, 55–69.
Shannon, R. D. (**1976**). "Revised effective ionic radii and systematic studies of interatomic distances in halides and chalcogenides," Acta Crystallogr. **A32**, 751–767.
Taylor, D. and Henderson, C. M. B. (**1968**). "The thermal expansion of the leucite group of minerals," Am. Mineral. **53**, 1476–1489.
van Laar, B. and Yelon, W. B. (**1984**). "The peak in neutron powder diffraction," J. Appl. Crystallogr. **17**, 47–54.
Yanase, I., Kobayashi, H., Shibasaki, Y., and Mitamura, T. (**1997**). "Tetragonal-to-cubic structural phase transition in pollucite by low-temperature X-ray powder diffraction," J. Am. Ceram. Soc. **80**, 2693–2695.